

seismic components, but they are evident for the 2004 Sumatra-Andaman earthquake.

48. T. C. Hanks, H. Kanamori, *J. Geophys. Res.* **84**, 2348 (1979).
49. S. Stein, M. Wysession, *An Introduction to Seismology, Earthquakes, and Earth Structure* (Blackwell Scientific, Malden, MA, 2003).
50. M. Ishii, P. Shearer, H. Houston, J. Vidale, *Nature*, in press.
51. R. Bilham, E. R. Engdahl, N. Feldt, S. P. Satyabala, *Seism. Res. Lett.*, in press.
52. Synthetics are computed according to normal-mode perturbation theory (16). Perturbations from a spherical nonrotating Earth model, such as rotation, ellipticity, and lateral heterogeneity are included. We adopt mantle model S2ORTS (53) and crustal model crust2.0 (54) to account for lateral heterogeneity. The latest estimates of spheroidal and toroidal eigenfrequencies and quality factors are used in the calculation (55). Modal splitting and coupling due to rotation, ellipticity, and lateral heterogeneity are accounted for on the basis of a group coupling scheme using 36 subgroups of 117 modes below 3 mHz (56).
53. J. Ritsema, H. J. van Heijst, *Sci. Prog. (New Haven)* **83**, 243 (2000).
54. C. Bassin, G. Laske, G. Masters, *Eos* **81** (Fall Meeting Suppl.), F897 (abstr. S21A-03) (2000).
55. The Reference Earth Model Web site is at <http://mahi.ucsd.edu/Gabi/rem.html>.
56. A. Duess, J. Woodhouse, *Geophys. J. Int.* **146**, 833 (2001).
57. R. Pillet, N. Florsch, J. Hinderer, D. Rouland, *Phys. Earth Planet. Inter.* **84**, 161 (1994).
58. S. Kedar, G. A. Hagi, B. D. Wilson, M. B. Heflin, *Geophys. Res. Lett.*, **30**, 1829, doi:10.1029/2003GL017639 (2003).
59. W. Zürn, R. Widmer, *Geophys. Res. Lett.* **22**, 3537 (1995).
60. M. Van Camp, *Phys. Earth Planet. Inter.* **116**, 81 (2000).
61. S. Rosat, J. Hinderer, L. Rivera, *Geophys. Res. Lett.*, **30**, 2111, doi:10.1029/2003GL018304 (2003).

62. This work was supported in part by NSF. Seismic waveform data from the Global Seismographic Network (funded by NSF and U.S. Geological Survey) were obtained from the Incorporated Research Institutions for Seismology (IRIS) Data Management System. Seismic waveform data was also obtained from the Geoscope Program (IPGP France) and the Southern California Earthquake Center.

Supporting Online Material

www.sciencemag.org/cgi/content/full/308/5725/1139/DC1

SOM Text
Figs. S1 to S5
Table S1

15 March 2005; accepted 29 April 2005
10.1126/science.1112305

REPORT

Periodically Triggered Seismicity at Mount Wrangell, Alaska, After the Sumatra Earthquake

Michael West,* John J. Sánchez, Stephen R. McNutt

As surface waves from the 26 December 2004 earthquake in Sumatra swept across Alaska, they triggered an 11-minute swarm of 14 local earthquakes near Mount Wrangell, almost 11,000 kilometers away. Earthquakes occurred at intervals of 20 to 30 seconds, in phase with the largest positive vertical ground displacements during the Rayleigh surface waves. We were able to observe this correlation because of the combination of unusually long surface waves and seismic stations near the local earthquakes. This phase of Rayleigh wave motion was dominated by horizontal extensional stresses reaching 25 kilopascals. These observations imply that local events were triggered by simple shear failure on normal faults.

After the great earthquake in Sumatra (1), local earthquakes spaced evenly in time occurred at Mount Wrangell, one of the world's largest andesite shield volcanoes. Located in south-central Alaska, Mount Wrangell anchors the eastern end of the Aleutian-Alaska chain of arc volcanoes (Fig. 1). Fumaroles, frequent seismicity, and historical steam plumes attest to Wrangell's active geothermal system (2). Because of its volcanic and seismic activity, a network of seismometers is jointly operated in the Wrangell area by the Alaska Volcano Observatory and the Alaska Earthquake Information Center. Surface waves from the moment magnitude (M_w) 9.0 Sumatra earthquake on 26 December 2004 propagated across the regional network and produced vertical trough-to-peak ground displacements of 1.5 cm. A swarm of 14 earthquakes near Mount Wrangell occurred during the passage of the Rayleigh waves (fig. S1), about 1 hour after the initial rupture in Indonesia (Fig. 2).

Six of the local events were large enough to be located. All of these were within 10 km of the summit caldera. The local signals were

strongest near the summit at station WANC, suggesting even tighter clustering. Determination of precise locations and focal mechanisms was inhibited by the emergent waveforms and the modest four-station local network. With one exception, located events occurred at depths of 2 km or less. Magnitudes ranged up to local magnitude 1.9. The variation in waveforms and amplitudes, and the scatter in event locations,

indicate that the triggered events were not coming from a single source but instead were dispersed around the summit. Some of the waveforms may be composites of more than one simultaneous event. Although 90% of the routinely located seismicity at Wrangell is of the long-period type (3), the events in the triggered cluster appear to have been high-frequency tectonic events (except for event 3, Fig. 2B).

Small earthquakes are common at Wrangell. A comparison to the two days before and after the Sumatra earthquake, however, shows a less than 1% probability of six randomly occurring events of any type in any 10-min window. This probability is further decreased by the requirement of magnitudes up to 1.9; high-frequency tectonic origin; even spacing between events; and coincident timing with teleseismic Rayleigh wave ground motion. Although these

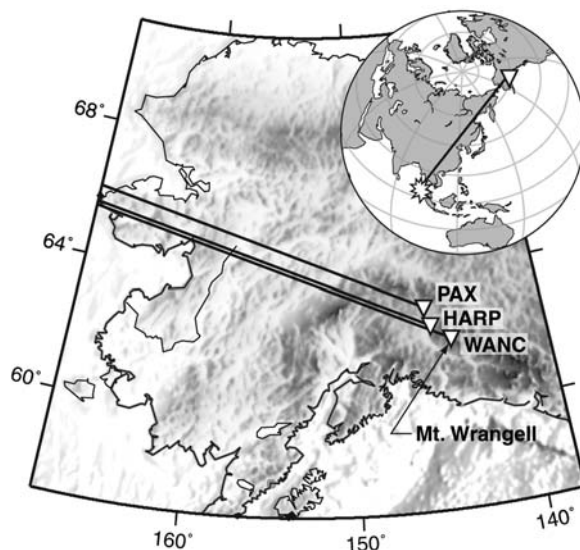


Fig. 1. Map with great circle paths from Sumatra to Mount Wrangell. Surface waves arrived at Wrangell from the west-northwest. Station WANC is at the summit of Wrangell. Three other short-period stations, including one three-component instrument (not shown), are located within 10 km of WANC. Stations PAX and HARP are nearby broadband instruments that are 115 and 72 km from WANC, respectively.

Alaska Volcano Observatory, Geophysical Institute, University of Alaska, Fairbanks, AK 99775, USA.

*To whom correspondence should be addressed.
E-mail: west@gi.alaska.edu

additional constraints are hard to quantify formally, they remove any doubt about whether the timing of the local swarm and the Sumatran event could be coincidence.

Remotely triggered seismic swarms in volcanic and geothermal regions have been documented after numerous earthquakes. The first well-documented example of widespread triggering was the 1992 M_w 7.3 Landers

earthquake, which initiated swarms at several locations in the western United States (4, 5). The M_w 7.9 Denali earthquake in 2002 triggered swarms at distances up to 4000 km (6). The recent Wrangell episode demonstrates that great earthquakes can perturb geothermal and volcanic systems around the world.

The hydrothermal system at Wrangell has a history of being disturbed by earthquakes (7).

The seismicity rate at Mount Wrangell dropped by 50% in the five months after the Denali earthquake (3). In the Denali case, static stress changes due to motion on the fault, less than 100 km away, present a plausible control on seismicity that cannot be invoked in the recent episode. No change in the seismicity rate has been observed since the Sumatra earthquake. Although different mechanisms may be at work in each period, the post-Denali changes indicate that the open hydrothermal system at Wrangell exists in a tenuous equilibrium.

The events at Mount Wrangell are distinguished from other remotely triggered swarms by the one-to-one correspondence between local earthquakes and cycles within the teleseismic wave train. All of the 14 Wrangell earthquakes that occurred during the passage of large-amplitude Rayleigh waves occurred during the same phase of the teleseismic waveform (Fig. 2B and fig. S2). The best comparison between local and teleseismic records was provided by station WANC (Fig. 2B). The 30-s surface waves were clearly recorded despite the 1-Hz natural frequency of the vertical short-period sensor. A formal instrument response correction was applied to the data. Conceptually, this correction consists of an amplification of several orders of magnitude and a phase shift of 180° for relatively long periods such as those described here (8). Because short-period instruments are not designed for interpreting teleseismic surface waves, we compared the corrected traces to nearby broadband instruments, each corrected for individual response. The broadband sensors were too far away to record the local swarm. They were essential, however, in verifying the short-period instrument response correction and providing more reliable ground motion amplitudes. This comparison demonstrates that the short-period instruments accurately captured the phase of the surface wave signal (Fig. 2D), despite a relative gain of less than 0.001 for 30-s periods relative to 1-s periods.

We compared the local events with the Sumatra earthquake by investigating the arrivals recorded at station WANC, with the caveat that event origin times may be 2 to 3 s earlier than their arrival times. A shift of 2 to 3 s will have a negligible effect on correlation with 20- to 30-s surface waves. We integrated the original velocity records to displacement for ease of visualization. All local events correlated with periods of positive vertical ground displacement. In addition, there is a correspondence between the amplitude of displacement and whether or not local events were triggered. Phases with amplitudes below 0.25 cm did not trigger events. Given the derivation described below, this corresponds to a threshold transient stress of ~ 8 kPa. An M_w 8.1 earthquake near the Macquarie Islands 3 days earlier produced stresses an order of magnitude lower and was not accompanied by anomalous earthquakes at Mount Wrangell.

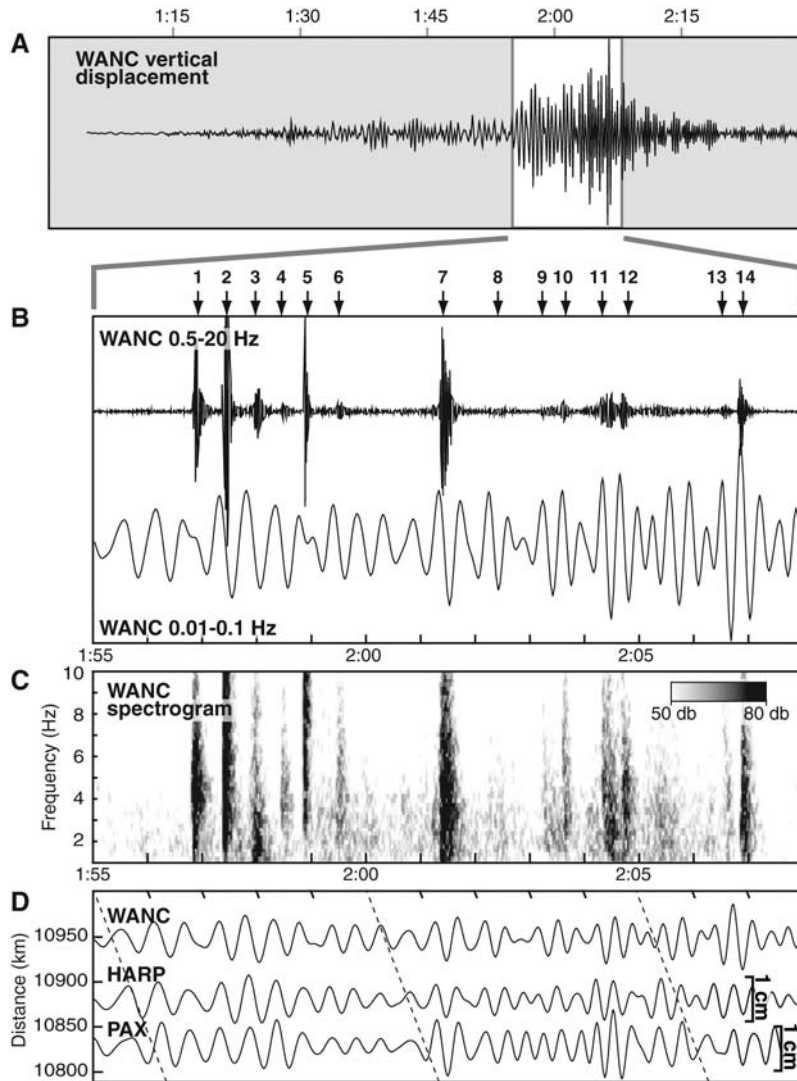


Fig. 2. Seismic records of the Sumatra earthquake and local events at Mount Wrangell. (A) Vertical component displacement record from short-period station WANC, plotted against universal time on 26 December 2004. Large-amplitude Rayleigh phases arrived in Alaska 1 hour after the Sumatra earthquake. (B) Expanded view of surface wave displacement at WANC. The upper record is filtered on 0.5 to 20 Hz to highlight high-frequency local earthquakes (indicated by numbers 1 to 14). The lower record is filtered instead on 0.01 to 0.1 Hz to show teleseismic ground motion. Large-amplitude vertical excursions of the teleseismic signal are correlated with the occurrence of local events. Estimates of true ground motion are unreliable at long periods for this short-period instrument. (C) Spectrogram showing frequency content of local events, obtained by applying a Fourier transform to 5-s windows of the WANC record. db, decibels. (D) Comparison of WANC displacement records to those from nearby broadband stations. Distances given are the distance to the station from the Sumatra earthquake epicenter. Dashed lines mark a time axis that has been skewed to adjust HARP and PAX records to appear as if they were recorded at WANC. HARP and PAX records are shifted by 24 and 37 s, respectively, corresponding to a velocity of 3.1 km/s. Scale bars mark the amplitude of displacement recorded at HARP and PAX. All three records show excellent phase correlation, affirming the reliability of short-period station WANC. The sensors at WANC, HARP, and PAX are a Mark Products L-4, a Güralp CMG-3T, and a Streckeisen STS-2, respectively.

The key to understanding these events was provided by nearby broadband, three-component seismometers that linked the events to teleseismic radial retrograde motion indicating Rayleigh waves (fig. S1). Shear and normal stresses work in tandem to promote faulting. Shear stresses alter the forces acting along fault planes, whereas normal stresses alter the confining pressure and friction across the faults. Although we do not know the orientation of faults deep within Mount Wrangell, analysis of the Rayleigh wave stress field can give insights into the faulting mechanism. We used a two-dimensional half-space model to estimate normal and shear stresses in the vertical and radial directions (9). We started with equations for particle displacement for a 30-s Rayleigh wave traveling with a phase velocity of 3.7 km/s. We calculated spatial derivatives to obtain strain and stress values across horizontal and vertical planes, using constitutive laws that assume a Poisson ratio of 0.25 and a shear modulus of 35 GPa (10) (figs. S1 to S3). The horizontal and vertical normal stresses, σ_{xx} and σ_{zz} , vary in phase with one another and are in phase with vertical ground displacement. Shear stresses σ_{xz} and σ_{zx} are out of phase by a quarter cycle and peak when the vertical displacement is 0. The exact stresses and depths vary greatly as a function of Rayleigh wave frequency and velocity structure. However, a few trends are clear. Near the surface, σ_{xx} is necessarily the only nonzero stress component (fig. S3). σ_{xx} diminishes with depth, whereas σ_{zz} increases until the two are equal in the mid-crust. The shear stresses, σ_{xz} and σ_{zx} , are zero at the surface and increase with depth. In a realistic Earth structure, stress concentrations will occur near subsurface boundaries; however, these basic trends remain. The events at Mount Wrangell occurred in the top few kilometers, suggesting that failure was controlled primarily by changes in the horizontal normal stress, σ_{xx} , which varied by up to ± 25 kPa. Specifically, the events occurred during periods of extensional horizontal stress.

The apparent instantaneous initiation of earthquakes during periods of positive ground displacement constrains the possible mechanisms for triggered seismicity. The correlation suggests that triggering is not due to a cumulative stress effect over many cycles. Rather,

the triggered events are the result of deformation over the preceding several seconds only. This is further confirmed by the observation that local events began immediately after the onset of large-amplitude Rayleigh wave displacements. Our favored explanation is simple shear failure. The correlation with extensional horizontal stress implies that the most favorable fault mechanisms are normal faults striking perpendicular to the direction of wave propagation (11). We do not have fault mechanism information to verify this possibility. However, the analysis of individual stress components provides a powerful tool for future studies in which fault mechanisms are known. Many different behaviors are encompassed under the broad label of triggering, and more than one mechanism is likely at work. In this case, however, the immediate failure of normal faults as a result of transient stresses can explain the features we observed.

An additional attraction to shear failure is its simplicity. In the case of Mount Wrangell, secondary effects involving fluid movement, bubbles, or crack weakening are not required. The events at Mount Wrangell occurred during phases of reduced confining pressure when faults were shifted closer toward failure. This does not explain how such minute stress changes are capable of stressing a fault to failure. After more than a decade of documented remote triggering episodes, it is clear that most occur in geothermal or volcanic systems, suggesting that high pore fluid pressures already maintain faults close to failure (12–15). The recent earthquakes are similar to prior triggering episodes in that high existing pore pressure may have primed fractures for failure in response to small transient stresses. The geothermal system at Mount Wrangell has a 50-year history of responding to large regional earthquakes and has demonstrated that small stress perturbations can drive substantial changes in fumarolic discharge (7).

Although the Mount Wrangell episode does not explicitly require the movement of pore fluids, a fluid pumping model may be compatible with our observations. In this model, a pressure increase squeezes fluids from interconnected pore space into nearby fault zones (16, 17). The assumption of an extensive hydrothermal system is reasonable in light of

persistent steam emissions from the summit of Mount Wrangell. Although increased pressure pumps the fluids according to Darcy's law, it is the total volume of fluid in the fault zone that would influence fault friction. The total fluid volume in the ensemble of fault zones is the integral of the flow. Thus, the maximum fluid content should lag roughly one-quarter phase behind the maximum pressure (Fig. 3). It is possible that such a fluid mechanism primes the fault zone, followed several seconds later by extensional stresses that trigger shear failure. The nonaligned phase relationship with triggered events, however, indicates that the fluid effect is a secondary factor, if it exists, and cannot solely explain the triggering.

The observations at Mount Wrangell are an especially clear case of what we suspect is a more general occurrence. The correlation was made clear by the unusually long-period surface waves and the close proximity of seismic stations. Analysis of existing data sets in light of this pattern may reveal phase correlation to be a powerful tool for identifying the mechanisms that control earthquake triggering.

References and Notes

1. J. Park *et al.*, *Science* **308**, 1139 (2005).
2. G. M. Cross, G. K. C. Clarke, C. S. Benson, *J. Geophys. Res.* **94**, 7237 (1989).
3. J. J. Sanchez, S. R. McNutt, *Bull. Seismol. Soc. Am.* **94**, S370 (2004).
4. D. P. Hill *et al.*, *Science* **260**, 1617 (1993).
5. J. S. Gombert, P. A. Reasenber, P. Bodin, R. A. Harris, *Nature* **411**, 462 (2001).
6. S. G. Prejean *et al.*, *Bull. Seismol. Soc. Am.* **94**, S348 (2004).
7. C. S. Benson, G. Bender, R. J. Motyka, A. B. Follett, *Eos* **76**, 198 (1995).
8. K. Aki, P. Richards, *Quantitative Seismology* (University Science Books, Sausalito, CA, ed. 2, 2002).
9. J. Gombert, S. Davis, *J. Geophys. Res.* **101**, 733 (1996).
10. Materials and methods are available as supporting material on Science Online.
11. C. Scholz, *The Mechanics of Earthquakes and Faulting* (Cambridge Univ. Press, Cambridge, ed. 2, 2002).
12. M. Cocco, J. R. Rice, *J. Geophys. Res.* **107**, 10.1029/2000JB000138 (2002).
13. S. Husen, S. Wiemer, R. B. Smith, *Bull. Seismol. Soc. Am.* **94**, S317 (2004).
14. J. E. Streit, S. F. Cox, *J. Geophys. Res.* **106**, 2235 (2001).
15. B. Sturtevant, H. Kanamori, E. E. Brodsky, *J. Geophys. Res.* **101**, 25 (1996).
16. E. E. Brodsky, E. Roeloffs, D. Woodcock, I. Gall, M. Manga, *J. Geophys. Res.* **108**, 10.1029/2002JB002321 (2003).
17. E. E. Brodsky, S. G. Prejean, *J. Geophys. Res.* **110**, 10.1029/2004JB003211 (2005).
18. This study was possible because of the combined seismic network efforts of the Alaska Volcano Observatory and the Alaska Earthquake Information Center. We also thank S. Prejean, J. Stachnik, J. Gombert, S. Moran, and two anonymous reviewers. Supported by National Science Foundation grant no. EAR-0326083 and by the Alaska Volcano Observatory, a cooperative program between the U.S. Geological Survey Volcano Hazards Program, the Geophysical Institute at the University of Alaska Fairbanks, and the Alaska Division of Geological and Geophysical Surveys.

Supporting Online Material

www.sciencemag.org/cgi/content/full/308/5725/1144/DC1
Materials and Methods
Figs. S1 to S3

18 March 2005; accepted 25 April 2005
10.1126/science.1112462

Fig. 3. Schematic showing the influence of trigger mechanisms relative to short- and long-period displacement records. The maximum extensional stresses are reached at the time of maximum vertical ground displacement. The secondary effect of high pore pressure due to fluid pumping into the fault zone may occur a quarter phase earlier. Although the flow into the fault zone peaks at the point of minimum displacement, the total volume of fluids in the fault would lag by roughly a quarter phase.

